Transactions on Machine Intelligence 6(2) (2023) 76-88

ISSN Online: 2821-1693

Transactions on Machine Intelligence

Journal Homepage: https://tmachineintelligence.ir/

Analytical Response of Nonlinear Buckling of Composite Plates Reinforced with Graphene Nanosheets

D. Shokri[1], M.R. Ebrahimian[2*], B. Tabibian[1], M.R. Allahverdlou[1], M.S. Atlasbaf[1]

[1] MSc Student, Department of Mechanics, Technical and Engineering Faculty, Imam Khomeini International University, Qazvin, Iran.
[2] Assistant Professor, Department of Mechanics, Technical and Engineering Faculty, Kar Higher Education Institute, Qazvin, Iran.

ARTICLE INFO

Article History:
Received 16 March 2023
Received in revised form
4 May 2023
Accepted 11 June 2023
Available online 12 June 2023

Keywords:
Composite, Reinforced With Graphene, Nonlinear Deformation, Buckling Load, Analytical Response

ABSTRACT

This paper presents a detailed analytical investigation into the nonlinear buckling behavior of a composite rectangular plate reinforced with graphene nanosheets (GNSs). The analysis is grounded in the third-order shear deformation theory (TSDT), which accurately captures transverse shear effects in thick plates. The governing equations are systematically derived using Hamilton's principle and result in a system of five coupled nonlinear partial differential equations. These equations are analytically solved using Navier's method, assuming simply supported boundary conditions along all four edges of the plate. The study explores the influence of key parameters including graphene distribution patterns, nanosheet geometry (thickness and width), the plate's thickness-to-length ratio, and the effects of geometric nonlinearity on the critical buckling load. To validate the analytical model, numerical results are compared with findings reported in the literature, demonstrating excellent agreement. The results highlight the significant reinforcement potential of GNSs in enhancing structural stability. Specifically, the inclusion of a small graphene content only 0.5% by mass can lead to a dramatic increase in the buckling load, nearly tripling it. These findings underscore the effectiveness of GNSs as nanofillers for improving the mechanical performance of composite structures under compressive loads, making them promising candidates for advanced engineering applications.

1. INTRODUCTION

This compilation of research articles explores advancements in the structural analysis of composite materials reinforced with graphene. The first article introduces a novel analytical approach for studying the buckling behavior of ring-stiffened porous graphene platelet-reinforced composite cylindrical shells under hydrostatic pressure [1]. The second article investigates the impact of increased graphene components and elastic foundation stiffness on the strength and buckling temperature of smart graphene/piezoelectric circular nanoplates [2]. The third article delves into the acoustic response of functionally graded graphene-reinforced composite plates under nonuniform edge

* Corresponding author: ebrahimian.reza@gmail.com
Assistant Professor, Department of Mechanics, Technical and Engineering Faculty, Kar Higher Education Institute, Qazvin, Iran

http://dx.doi.org/10.47176/TMI.2023.76

loads, emphasizing the significance of aspect ratio [3]. Lastly, the fourth article focuses on the influence of graphene-platelets on the natural frequency and thermal buckling temperature of annular sandwich plates, providing insights into vibration and symmetric thermal buckling behaviors [4].

With the growing development of era and production strategies and the opportunity of manufacturing included parts, the research and evaluation of composite and bolstered systems have received unique importance. Reinforced systems, which include beams, sheets and shells, are extensively utilized in industries together with vehicles and aerospace. These systems have excessive energy and mild weight on the identical time and feature higher static and dynamic conduct. Designing a bolstered shape consistent with its overall performance requires static and buckling analyses.

Javaheri and Eslami [5] have investigated the linear buckling conduct of a square sheet made from graded cloth with an energy characteristic of the usage of the classical concept of skinny sheets. Asmi et al. [6] have analyzed the buckling of a square sheet made from graded cloth of the energy version the usage of the finite detail technique is primarily based totally on the concept of three-dimensional deformation.

Due to the lengthy records of the usage of bolstered sheets, many specific types of research have been completed up to now to reap greater green strategies and greater correct answers. Golmakani and Zaighami [7] analyzed buckling in bolstered composite sheets. had been completed with the graded distribution of carbon nanotubes alongside the thickness. They received the governing equations by thinking about the first-order shear concept of Van Karman nonlinear lines and calculated the essential load of sheet buckling through the dynamic launch technique. Zhao and Kapania [8] provided a way to outline the geometry of the curved reinforcement with the assistance of Nerbez features and simulated the buckling inside the composite bolstered sheet with the usage of the finite detail technique. The benefit of their proposed technique is that through converting the geometry of the amplifier, there may be no want to re-grid, that's an essential benefit in fixing problems.

Also some papers collectively explore various facets of structural analyses and stability considerations in diverse materials:

In "Static and Dynamic Analyses of Isogeometrics Curvilinearly Stiffened Plates" [9], Qin et al. delve into mathematical modeling applications for isogeometric curvilinearly stiffened plates. "Isogeometric Buckling Analysis of Composite Variable-Stiffness Panels" [10], by Hao et al., contributes to understanding the buckling behavior of composite variable-stiffness panels through isogeometric analysis. Zamani's work [11], "Reinforcing Effect of Nanoclay on Buckling Behavior of Nanocomposite Grid Shells: Experimental Investigation," explores experimental investigations into the buckling behavior of nanocomposite grid shells reinforced with nanoclay. Mohammadi Mehr et al. in "Buckling and Vibration Analyzes of Double-Bonded Micro Composite Plates Reinforced by CNTs and BNNTs Based on MSGT" [12] use MSGT to analyze the buckling and vibration behavior of double-bonded micro composite plates reinforced with CNTs and BNNTs. "Static Stability of Higher Order Functionally Graded Beam under Variable Axial Load" [13], authored by Melaibari et al., investigates the static stability of higher-order functionally graded beams under variable axial loads, emphasizing the structural stability aspects.

Karamanelli and Aidoglou [14] analyzed the buckling of composite beams subjected to extensive axial loads with varying distribution patterns using the Ritz method. They found that the critical load was similar in magnitude to the load distribution modes for unique boundary conditions. Additionally, they explored the influence of the beam's length-to-thickness ratio and composite fiber orientation on the critical load. In a separate study, Dong et al. [15] investigated the buckling behavior of reinforced porous FGM cylindrical shells. The authors utilized the first-order shear theory of shells, accounting for changes in properties only through the thickness and radial direction of the shell. Alongside this approach, they employed the Galerkin technique with customized weight functions for varying boundary conditions. Jehwan et al. [16] investigated the nonlinear buckling behavior of reinforced and porous FG sheets. Donnell's theory, along with first-order shear deformation theory, was used to derive the governing equations. Donnell's theory, along with first-order shear deformation theory, was used to derive the governing equations. The Galerkin technique was then applied to solve these equations.

In a study of delamination in composites with varying degrees of hardness, Yazdani et al. [17] utilized the first-order shear deformation theory to model multilayer composites. Donnell's theory, along with first-order shear deformation theory, was used to derive the governing equations. The advanced finite element method was employed

to describe discontinuities. Penghao et al. [18] conducted an objective analysis of the buckling of composite plates with variable stiffness, utilizing isometric evaluation based on the first-order shear deformation theory. Technical term abbreviations were explained upon first use. The text features a clear structure with a logical flow of information with causal connections between statements. In a similar study, Manicom et al [19] investigated the thermal buckling of composite sheets with variable hardness under thermal load employing finite elements based on the first-order shear deformation theory. Biased, emotional, figurative, or ornamental language is avoided, and positions on subjects are conveyed through hedging. Both studies analyzed the behavior of uniform and non-uniform temperature distribution plates. The text adheres to conventional structure with factual and unambiguous titles, clear and objective language, and precise word choice. The format complies with style guides and consistent citation practices. The language is formal and free from grammatical errors, spelling mistakes, and punctuation errors.

In the beyond research, till now, the evaluation of the buckling crucial load of composite square plates bolstered with graphene nanosheets and in absolutely precise boundary conditions, the use of the idea of 0.33 order shear deformation and Van Karman pressure relations, has now no longer been said analytically; In this research, we are seeking for to do this.

2. ANALYTICAL MODELING

As seen in Fig.1, A rectangular nanocomposite sheet with specified dimensions, with three different forms of nanographene distribution is considered.

2.1. Sheet displacement field and strain components

The sheet displacement field using the theory of third order shear deformation is:

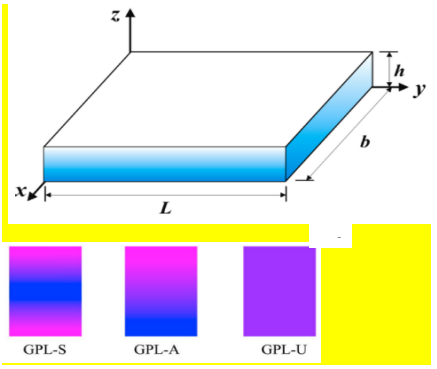

Fig. 1: A geometric representation of a rectangular sheet with various graphene thickness distributions

$$u_1(x,y,z;t)=u_0(x,y;t)-zw_{0,x}+[f(z)]\theta_x(x,y;t)$$
$$u_2(x,y,z;t)=v_0(x,y;t)-zw_{0,y}+[f(z)]\theta_y(x,y;t) \quad (1)$$
$$u_3(x,y,z;t)=w_0(x,y;t)$$

In the above relationship, $f(z)$ expresses the distribution function of the strain and transverse shear stresses along the cross-section, which for the theory of the third order deformation is equal to: $f(z)=z-\frac{4z^3}{3h^2}$. The non-zero components of sheet strain are presented in terms of displacement field components according to the following relations:

$$\begin{Bmatrix}\varepsilon_{xx}\\ \varepsilon_{yy}\\ \varepsilon_{xy}\end{Bmatrix}=\begin{Bmatrix}\varepsilon^0_{xx}\\ \varepsilon^0_{yy}\\ \varepsilon^0_{xy}\end{Bmatrix}-z\begin{Bmatrix}w_{0,xx}\\ w_{0,yy}\\ 2w_{0,xy}\end{Bmatrix}+[f(z)]\begin{Bmatrix}\theta_{0,xx}\\ \theta_{0,yy}\\ \theta_{x,y}+\theta_{y,x}\end{Bmatrix} \quad (2)$$
$$\begin{Bmatrix}\varepsilon_{xz}\\ \varepsilon_{yz}\end{Bmatrix}=[f(z)_{,z}]\begin{Bmatrix}\theta_x\\ \theta_y\end{Bmatrix}$$

The non-linear components of the strain are created due to the stretching of the middle plane and are:

$$\varepsilon_{xx}^{0}=u_{0,x}+0.5\,w_{0,x}^{2}$$
$$\varepsilon_{yy}^{0}=v_{0,y}+0.5\,w_{0,y}^{2} \quad (3)$$
$$\varepsilon_{xy}^{0}=u_{0,y}+v_{0,y}+w_{0,x}w_{0,y}$$

On the other hand, sheet stresses will be calculated according to the following equation:

$$\{\sigma_{xx} \quad \sigma_{yy} \quad \sigma_{xy} \quad \sigma_{xz} \quad \sigma_{yz}\}^{T}=[C]\,\boldsymbol{\varepsilon}^{T} \quad (4)$$

where [C] is the stiffness of the composite material, which is equal to:

$$[C]=\begin{bmatrix} \frac{E(z)}{1-v^2} & \frac{vE(z)}{1-v^2} & 0 & 0 & 0 \\ \frac{vE(z)}{1-v^2} & \frac{E(z)}{1-v^2} & 0 & 0 & 0 \\ 0 & 0 & \frac{E(z)}{2(1+v)} & 0 & 0 \\ 0 & 0 & 0 & \frac{E(z)}{2(1+v)} & 0 \\ 0 & 0 & 0 & 0 & \frac{E(z)}{2(1+v)} \end{bmatrix} \quad (5)$$

1.2 Composite reinforced with graphene sheets

Figure 1 illustrates the distribution of Grafted Polymer Layers (GPLs) in three distinct distribution types. It is evident from the figure that the Volume Fraction of GPLs (VGPL) undergoes continuous changes throughout the shell thickness in the GPL-A and GPL-S samples, whereas it is uniformly distributed in the GPL-U sample. We hypothesize that the nanoscale fillers in GPLs are intertwined with the matrix. Then, we describe the following features to define the distribution of Generalized Pareto distributions in these three modes, utilizing the $\Theta_i$values [20].

$$\text{GPL-U: } \Theta_1(z)=1$$
$$\text{GPL-S:}\Theta_2(z)=1-\cos\left(\frac{\pi z}{h_c}\right) \quad (6)$$
$$\text{GPL-A:}\Theta_3(z)=1-\cos\left(\frac{\pi z}{2h_c}+\frac{\pi}{4}\right)$$

The relationship between the shape function and the volume fraction of VGPL, GPL is $V_{GPL}(z) = S_i\Theta_i(z)$. To establish a relationship between the volume fraction and the mass fraction G of the reinforcement phase and to find the values of Si, the following equation can be written for the reinforced porous composite [21]:

$$\frac{G}{G+(\rho_{GPL}/\rho_m)(1-G)}=\frac{S_i}{h}\int_{-h/2}^{h/2}\Theta_i(z)dz \quad (7)$$

The geometric dimensions of graphene platelets (GPLs) can affect the Young's moduli of GPL-reinforced mixes. To calculate the applicable Young's moduli compared to the law of combinations, we opted for the improved Halpin-Say micromechanical model, which was validated by the work of MARafiee et al. [22]. The law of combinations can be used to estimate Poisson's rate and applicable viscosity. Micromechanics proposition has been employed to predict the applicable thermal conductivity measurement of the new compound.

$$E_c(\zeta)=E_m\left[\frac{3}{8}\left(\frac{1+2\xi_L\eta_L V_{GPL}}{1-\eta_L V_{GPL}}\right)+\frac{5}{8}\left(\frac{1+2\xi_B\eta_B V_{GPL}}{1-\eta_B V_{GPL}}\right)\right]$$
$$\upsilon_c(\zeta)=\upsilon_{GPL}V_{GPL}+\upsilon_m(1-V_{GPL}) \quad (8)$$
$$\rho_c(\zeta)=\rho_{GPL}V_{GPL}+\rho_m(1-V_{GPL})$$

where the subscripts GPL and m represent the parcels of GPL corresponding to the material and the background matrix of the external aeroplanes, independently. Other GPL parameters are also expressed by the following relations, that L_{GPL}, b_{GPL} and t_{GPL} are the average length, range and consistence of GPL, independently.

$$\begin{aligned} \xi_L &= \frac{L_{GPL}}{t_{GPL}}, \quad \eta_L = \frac{E_{GPL}-E_m}{E_{GPL}-\xi_L E_m} \\ \xi_B &= \frac{b_{GPL}}{t_{GPL}}, \quad \eta_B = \frac{E_{GPL}-E_m}{E_{GPL}-\xi_B E_m} \end{aligned} \tag{9}$$

3. HAMILTON'S PRINCIPLE AND EQUILIBRIUM EQUATION

To reach the equilibrium equations of the compound distance under the effect of internal loads, Hamilton's principle is used according to the following equation:

$$\int_{t_1}^{t_2} (\delta U - \delta V)\,dt = 0 \tag{10}$$

where δU is the virtual change of strain energy of the system and δV is the virtual change of work done by external forces. These expressions can be expressed with the following equations:

$$\begin{aligned} \delta U &= \int_{\Omega_0}^{/} \int_{-h/2}^{h/2} \left[\sigma_{xx}\delta\varepsilon_{xx}+\sigma_{yy}\delta\varepsilon_{yy}+\sigma_{xy}\delta\varepsilon_{xy}+\sigma_{xz}\delta\varepsilon_{xz}+\sigma_{yz}\delta\varepsilon_{yz}\right] dz\,dx\,dy \\ \delta V &= \int_{\Omega_0}^{*} (\bar{N})\delta w_0\,dx\,dy \end{aligned} \tag{11}$$

Where Ω_0 is the cross section of the compound distance. $\bar{N}$ is also the external in- airplane force.

also, the results of force, necklace and high order results of stress are attained according to the following relations:

$$\left[N_{ij},\quad M_{ij},\quad H_{ij},\quad J_{ij}\quad \rho\right] = \int_{-h/2}^{h/2} Q_{ij}\,[1,\quad z,\quad f(z),\quad f(z)_{,z}\quad \rho]\,dz\ ;\ (i,j=x,y,z) \tag{12}$$

In the following, the relations of changes in the strain energy of the system according to the results of the stress introduced below are presented as follows:

$$\begin{aligned} \delta U \quad = \int_{\Omega_0}^{*} [& N_{xx}(\delta u_{0,x} + w_{0,x}\delta w_{0,x}) - M_{xx}\delta w_{0,xx} + (H_{xx})\delta\theta_{x,x} \\ & + N_{yy}\left(\delta v_{0,y} + w_{0,y}\delta w_{0,y}\right) - M_{yy}\delta w_{0,yy} + \left(H_{yy}\right)\delta\theta_{y,y} \\ & + N_{xy}\left(\delta u_{0,y} + \delta v_{0,x} + w_{0,y}\delta w_{0,x} + w_{0,x}\delta w_{0,y}\right) - 2M_{xy}\delta w_{0,xy} \\ & + \left(H_{xy}\right)\left(\delta\theta_{x,y} + \delta\theta_{y,x}\right) + \left(J_{x,z}\right)\delta\theta_x + \left(J_{y,z}\right)\delta\theta_y]\,dx\,dy \end{aligned} \tag{13}$$

On the other hand, the changes in the work of external in- aeroplane forces are also:

$$\delta V = \int_{\Omega_0}^{*} \bar{N}\,\delta w_0\,dx\,dy \tag{14}$$

By placing the below relations in Hamilton's principle and performing part by part integration, the sum of the portions related to different terms, five nonlinear buckling balance equations for the distance are attained in terms of stress results:

$$\begin{aligned} & N_{xx,x}+N_{xy,y}=0 \\ & N_{yy,y}+N_{xy,x}=0 \\ & N_{xx,x}w_{0,x} + N_{xx}w_{0,xx} + N_{yy,y}w_{0,y} + N_{yy}w_{0,yy} + N_{xy,x}w_{0,y} + N_{xy,y}w_{0,x} + 2N_{xy}w_{0,xy} \\ & \qquad + M_{xx,xx} + M_{yy,yy} + 2\,M_{xy,xy} + \bar{N} = 0 \end{aligned} \tag{15}$$

$$H_{xx,x}+H_{xy,y}-J_{xz}=0$$
$$H_{yy,y}+H_{xy,x}-J_{yz}=0$$

The discriminational equations of distance balance in terms of distance relegation factors and cross-sectional stress results, using Hamilton's principle, are according to the following five equations:

$$A_{11}\left(u_{0,xx}+w_{0,x}w_{0,xx}\right)-B_{11}w_{0,xxx}+(E_{11})\theta_{x,xx}+A_{12}\left(v_{0,xy}+w_{0,y}w_{0,xy}\right)-B_{12}w_{0,xyy}$$
$$+(E_{11})\theta_{y,xy}+A_{44}\left(u_{0,yy}+v_{0,xy}+w_{0,x}w_{0,yy}+w_{0,xy}w_{0,y}\right)-2B_{44}w_{0,xyy}+(E_{44})\left(\theta_{x,yy}+\theta_{y,xy}\right)=0 \quad (16)$$

$$A_{22}\left(u_{0,yy}+w_{0,y}w_{0,yy}\right)-B_{22}w_{0,yyy}+(E_{22})\theta_{y,yy}+A_{12}\left(v_{0,xy}+w_{0,x}w_{0,xy}\right)-B_{12}w_{0,xxy}+(E_{12})\theta_{x,xy}$$
$$+A_{44}\left(u_{0,xy}+v_{0,xx}+w_{0,x}w_{0,xy}+w_{0,xx}w_{0,y}\right)-2B_{44}w_{0,xxy}+(E_{44})\left(\theta_{x,xy}+\theta_{y,xx}\right)=0$$

$$w_{0,xx}\left[A_{11}\left(u_{0,x}+\frac{1}{2}w_{0,x}^2\right)-B_{11}w_{0,xx}+(E_{11})\theta_{x,x}-T_{11}+A_{12}\left(v_{0,y}+\frac{1}{2}w_{0,y}^2\right)-B_{12}w_{0,yy}+(E_{12})\theta_{y,y}-T_{12}\right]+w_{0,yy}\left[A_{22}\left(u_{0,y}+\frac{1}{2}w_{0,y}^2\right)-B_{22}w_{0,yy}+(E_{22})\theta_{y,y}-T_{22}+A_{12}\left(v_{0,x}+\frac{1}{2}w_{0,x}^2\right)-B_{12}w_{0,xx}+(E_{12})\theta_{x,x}-T_{12}\right]+2w_{0,xy}[A_{44}\left(u_{0,y}+u_{0,x}+w_{0,x}w_{0,y}-2B_{44}w_{0,xy}+(E_{44})\left(\theta_{x,y}+\theta_{y,x}\right)\right]+B_{11}\left(u_{0,xxx}+w_{0,xx}^2+w_{0,x}w_{0,xxx}\right)-D_{11}w_{0,xxxx}+(F_{11})\theta_{x,xxx}+B_{12}\left(u_{0,xxy}+w_{0,xy}^2+w_{0,y}w_{0,xxy}\right)-D_{12}w_{0,xxyy}+(F_{12})\theta_{y,xxy}+B_{22}\left(u_{0,yyy}+w_{0,yy}^2+w_{0,y}w_{0,yyy}\right)-D_{22}w_{0,yyyy}+(F_{22})\theta_{y,yyy}+B_{12}\left(u_{0,xyy}+w_{0,xy}^2+w_{0,x}w_{0,xyy}\right)-D_{12}w_{0,xxyy}+(F_{12})\theta_{x,xyy}+2B_{44}\left(u_{0,xyy}+u_{0,xxy}+w_{0,xy}^2+w_{0,x}w_{0,xyy}+w_{0,xxy}w_{0,y}+w_{0,xx}w_{0,yy}\right)-4D_{44}w_{0,xxyy}+2(F_{44})\left(\theta_{x,xyy}+\theta_{y,xxy}\right)+\bar{N}=0 \quad (17)$$

$$(E_{11})\left(u_{0,xx}+w_{0,x}w_{0,xx}\right)-(F_{11})w_{0,xxx}+(I_{11})\theta_{x,xx}+(E_{12})\left(v_{0,xy}+w_{0,y}w_{0,xy}\right)-(F_{12})w_{0,xyy}+(I_{12})\theta_{y,xy}+(E_{44})\left(u_{0,xx}+v_{0,xy}+w_{0,xy}w_{0,y}+w_{0,x}w_{0,yy}\right)-2(F_{44})w_{0,xyy}+(I_{44})(\theta_{x,yy}+\theta_{y,xy})-(S_{44})\theta_x=0 \quad (18)$$

$$(E_{22})\left(u_{0,yy}+w_{0,y}w_{0,yy}\right)-(F_{22})w_{0,yyy}+(I_{22})\theta_{y,yy}+(E_{12})\left(u_{0,xy}+w_{0,x}w_{0,xy}\right)-(F_{12})w_{0,xxy}+(I_{12})\theta_{x,xy}+(E_{44})\left(u_{0,xy}+v_{0,xx}+w_{0,xx}w_{0,y}+w_{0,x}w_{0,xy}\right)-2(F_{44})w_{0,xxy}+(I_{44})(\theta_{x,xy}+\theta_{y,xx})-(S_{44})\theta_y=0 \quad (19)$$

In these five equations, the coefficients related to the cross section are equal to:

$$\left[A_{ij}\quad B_{ij}\quad D_{ij}\quad E_{ij}\quad F_{ij}\quad I_{ij}\quad K_{ij}\quad S_{ij}\right]=\int_{-h/2}^{h/2}Q_{ij}\left[1\quad z\quad z^2\quad f(z)\quad zf(z)\quad f^2(z)\quad f(z)_{,z}\quad (f(z)_{,z})^2\right]dz\ ;\ (i,j=1,2,4) \quad (20)$$

4. SOLVING NONLINEAR COUPLE EQUILIBRIUM EQUATIONS

Navier's method was utilized to obtain a logical solution to the nonlinear equations of the compound distance buckling problem. It is assumed that the four supports of the distance are articulated and the deflection fields of the distance can be expressed as trigonometric functions and indefinite fractions to fulfill the boundary conditions. Objective evaluation has been incorporated throughout. Additionally, conventional formatting and clear, precise language were maintained, formal register employed, and grammar checked to ensure accuracy. Quotations are clearly marked and filler words avoided. The text adheres to established academic structure with a logical flow of information that includes causal connections between statements.

$$\begin{Bmatrix}u_0\\v_0\\w_0\\\theta_x\\\theta_y\end{Bmatrix}=\sum_{n=1}^{\infty}\sum_{m=1}^{\infty}\begin{Bmatrix}r_{mn}\cos\lambda_x x\sin\lambda_y y\\s_{mn}\sin\lambda_x x\cos\lambda_y y\\a_{mn}\sin\lambda_x x\sin\lambda_y y\\x_{mn}\cos\lambda_x x\sin\lambda_y y\\y_{mn}\sin\lambda_x x\cos\lambda_y y\end{Bmatrix} \quad (21)$$

where $\{r_{mn}\quad s_{mn}\quad a_{mn}\quad x_{mn}\quad y_{mn}\}^T$ is the vector of generalized portions of the factors of the relegation field in the distance and we have:

$$\lambda_x=m\pi/a\ ,\lambda_y=n\pi/b \quad (22)$$

In addition, the in-plane external force can be written in the following form [23]:

$$\bar{N}=N^0_{xx}w_{0,xx}+N^0_{yy}w_{0,yy} \tag{23}$$

whereN^0_{xx} and N^0_{yy} are the in-plane forces acting on the middle plane passing through the middle of the distance consistence in the x and y directions, independently, now we assume that N_{cr} is the critical buckling force, which applies in the following relations:

$$\begin{aligned} N^0_{xx}&=\gamma_x N_{cr}\\ N^0_{yy}&=\gamma_y N_{cr}\end{aligned} \tag{24}$$

Thus, when the condition $(\gamma_x,\gamma_y)=(-1,0)$ is established, the problem of the compressive force state is unidirectional, and while $(\gamma_x,\gamma_y)=(-1,-1)$ the expression The compressive force is bidirectional with the same quantum of force in each direction.

Eventually, by placing the connections of the stress results in the equilibrium equations and also considering the general form of the relegation field factors, the matrix form of the nonlinear equilibrium equations related to distance buckling can be written in the following form:

$$l0[Y]\begin{Bmatrix} r_{mn}\\ s_{mn}\\ a_{mn}\\ x_{mn}\\ y_{mn}\end{Bmatrix}-X_{nl}\begin{Bmatrix} 0\\ 0\\ a_{mn}{}^3\\ 0\\ 0\end{Bmatrix}=0 \tag{25}$$

The square matrix [Y] is symmetric with 5 rows and 5 columns, whose non-zero elements are:

$$\begin{aligned}
&Y_{11}=A_{11}\lambda_x^2+A_{44}\lambda_y^2\\
&Y_{12}=(A_{12}+A_{44})\lambda_x\lambda_y\\
&Y_{13}=-B_{11}\lambda_x^3-(B_{12}+2B_{44})\lambda_x\lambda_y^2\\
&Y_{14}=-E_{11}\lambda_x^2-(E_{44})\lambda_y^2\\
&Y_{15}=(E_{12}+E_{44})\lambda_x\lambda_y\\
&Y_{22}=A_{22}\lambda_y^2+A_{44}\lambda_x^2\\
&Y_{23}=-B_{22}\lambda_y^3-(B_{12}+2B_{44})\lambda_x^2\lambda_y\\
&Y_{24}=Y_{15}\\
&Y_{25}=E_{22}\lambda_y^2+(E_{44})\lambda_x^2\\
&Y_{33}=D_{11}\lambda_x^4+D_{22}\lambda_y^4+(2D_{12}+4D_{44})\lambda_x^2\lambda_y^2+N_{cr}(\eta_x\lambda_x^2+\eta_y\lambda_y^2)\\
&Y_{34}=-(F_{11})\lambda_x^3-(F_{12}+2F_{44})\lambda_x\lambda_y^2\\
&Y_{35}=-(F_{22})\lambda_y^3-(F_{12}+2F_{44})\lambda_x^2\lambda_y\\
&Y_{44}=(I_{11}\lambda_x^2+I_{44}\lambda_y^2)\\
&Y_{45}=(I_{12}+I_{44})\lambda_x\lambda_y\\
&Y_{55}=\left(I_{22}\lambda_y^2+I_{44}\lambda_x^2\right)+S_{44}
\end{aligned} \tag{26}$$

On the other hand, X_{nl} is the numerical coefficient of the nonlinear vector and consists of:

$$\begin{aligned}
X_{nl}=\big[&A_{11}\mathrm{sscc}(\lambda_x).\mathrm{sscc}(\lambda_y).\lambda_x^4+A_{12}.\mathrm{ssss}(\lambda_x).\mathrm{sscc}(\lambda_y).\lambda_x^2\lambda_y^2\\
&+A_{11}.\mathrm{ssss}(\lambda_x).\mathrm{sscc}(\lambda_y).\lambda_y^4+A_{12}.\mathrm{sscc}(\lambda_x).\mathrm{ssss}(\lambda_y).\lambda_x^2\lambda_y^2\\
&-4\times A_{44}.\mathrm{sscc}(\lambda_x).\mathrm{sscc}(\lambda_y).\lambda_x^2\lambda_y^2\big]/\big[2\mathrm{ss}(\lambda_x)\mathrm{ss}(\lambda_y)\big]
\end{aligned} \tag{27}$$

$$\begin{aligned}
&\mathrm{sscc}(\chi)=-\left(2\sin(\chi\pi)\cos^3(\chi\pi)-\cos(\chi\pi)\sin(\chi\pi)-\chi\pi\right)\\
&\mathrm{ssss}(\chi)=-\left(2\sin^3(\chi\pi)\cos(\chi\pi)-3\cos(\chi\pi)\sin(\chi\pi)-\chi\pi\right)/4\chi\\
&\mathrm{ss}(\chi)=-(\sin(\chi\pi)\cos(\chi\pi)\chi\pi)/\chi
\end{aligned}$$

5. NUMERICAL RESULTS

The confirmation of the results related to the critical cargo of direct buckling for the functional canted distance of aluminum/ alumina in terms of megapascals, with the confines a = 0.25 m, b = 0.5 m and the power parameter, p=1, has been done in Table 1.

Table 1. Validation of the results of linear buckling in the present analysis with the results of previous articles

Load type	Analysis method	a/h			
		5	10	20	40
Uniaxial	CPT [5]	267.480	33.435	4.1794	0.5224
	3D FEM [6]	237.988	32.332	4.1289	0.5195
	TSDT	239.145	32.472	4.1486	0.5215
Biaxial	CPT [5]	213.991	26.748	3.4353	0.4179
	3D FEM [6]	190.386	25.868	3.3071	0.4162
	TSDT	191.316	25.978	3.3189	0.4172

The mechanical properties of the matrix polymer and reinforced graphene are presented below:
E_m=3Gpa;ν_m=0.34;ρ_m=1200 Kg/m^3; E_{GPL}=1.01Tpa;ν_{GPL}=0.186;ρ_{GPL}=1062 $\frac{Kg}{m^3}$; l_{GPL}=2.5μm;w_{GPL}=1.5μm;t_{GPL}=2.5nm;

The dimensions of the page, if there is no change in the parametric analysis, are equal to $a = 20cm; b/a = 1.5; \delta = a/h = 5;$:

The effect of graphene distribution on the nonlinear buckling load and the ratio of nonlinear to direct buckling load for G = 1 is shown in Figure 2. According to Figure 2A, symmetrical and asymmetrical distributions have the highest and lowest critical buckling loads independently. The critical direct buckling load values of symmetric, asymmetric and invariant forms are equal to 20.87, 12.14 and 16.18 MPa, independently, and for this quantum of corroborated graphene, the direct buckling load of symmetric distribution is1.72 and1.29, independently. It's equal to the direct buckling load of asymmetric distribution and invariant distribution. On the other hand, according to Figure 2b, the distance buckling has the most nonlinear behavior.

The effect of the mass bit of graphene with symmetric distribution on the critical load nonlinear deformation and the rate of nonlinear to direct critical load is shown in Figure 3. As expected, the buckling critical load is advanced and the distortion is reduced as the quantum of underpinning graphene increases up to 1 mass. On the other hand, the nonlinear behavior is less in a section with further graphene; because the section with an advanced mass chance of graphene is harder. The direct buckling load was as shown PL =3.972, 8.507, 12.73, 20.87, in Figure 3a for G =0, 0.25%, 0.5%, 1% independently. The effect of graphene can be seen by adding the buckling load of the distance, so that with an increase of 0.5 of the mass of graphene, the buckling load has increased by 1/3. The critical load - nonlinear deformation at different values of consistence and range of graphene nanosheet is shown in Figure 4. At a fixed length, increasing the consistence and decreasing the range of graphene were the factors that increased the critical buckling load.

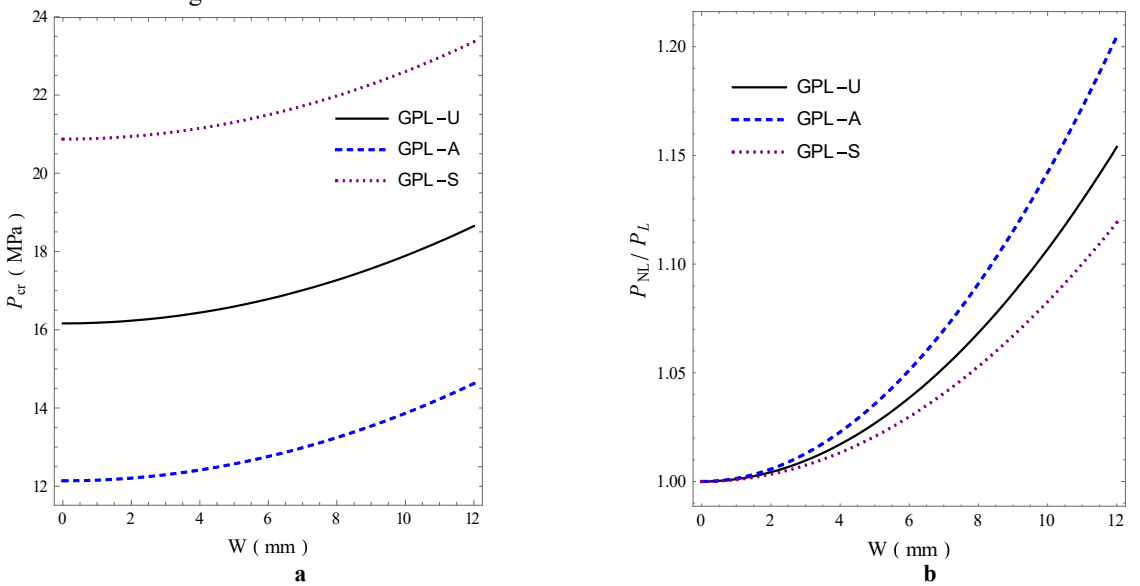

Fig. 2. The effect of graphene distribution on: a) critical load curve - nonlinear deformation; b) Non-linear to linear critical load ratio

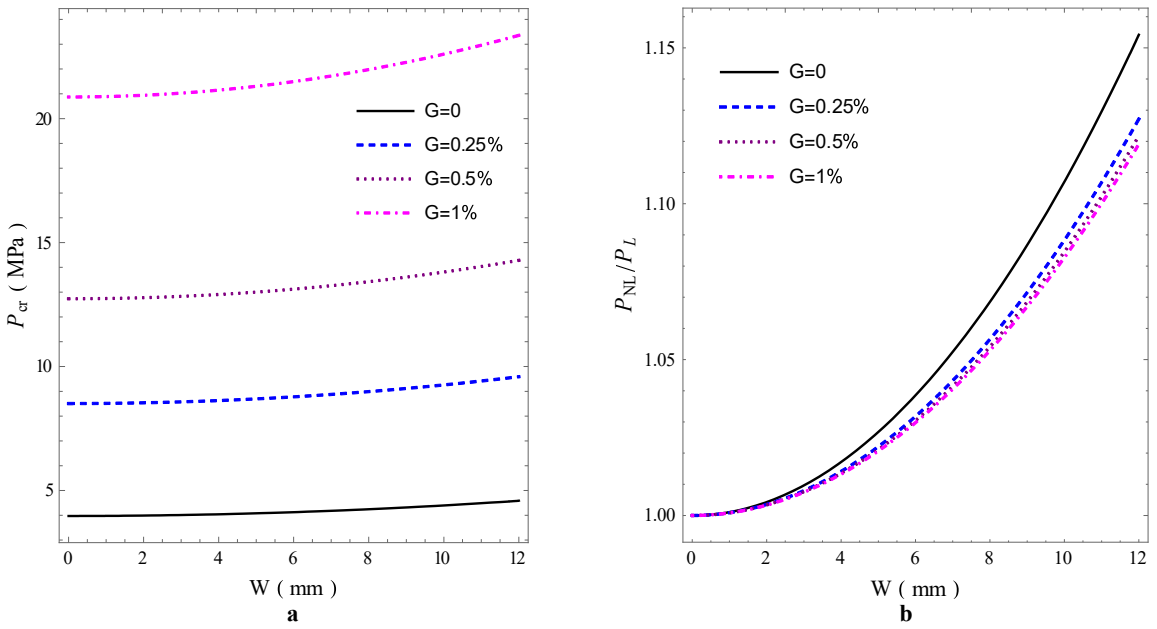

Fig. 3. The effect of graphene mass fraction on: a) critical load curve - nonlinear deformation; b) Non-linear to linear critical load ratio

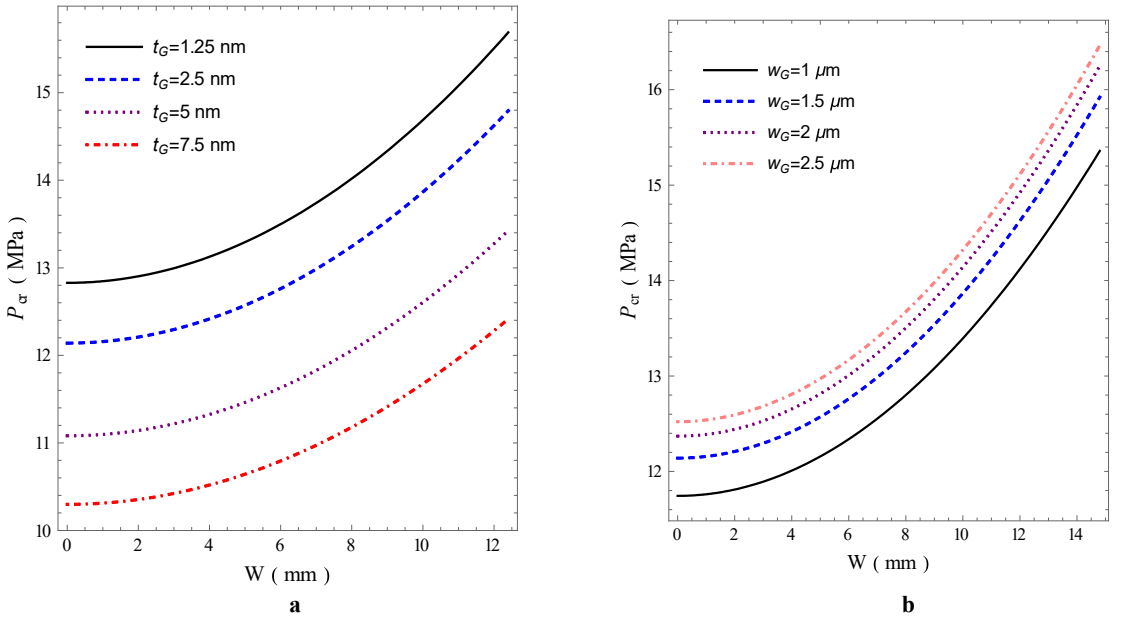

Fig. 4. Critical load curve - Deformation after buckling in different values: a(Graphene thickness; b) Graphene width

The effect of the ratio of the length to the thickness of the sheet The critical load curve - nonlinear deformation and the ratio of nonlinear to linear critical load in the case where the distribution of graphene is uniform and G = 0.5% is shown in Figure 5. With the length of the sheet remaining the same, the thinner the sheet) $\delta$the larger the parameter,(the lower the critical buckling load, while its nonlinear deformation is evident. According to Figure 5 a, the linear buckling load for is $\delta = 4,8$equal to $P_L = 18.17,2.699$and thus doubling the thickness of the nanocomposite plate has led to an 85% reduction in the critical buckling load in the linear mode.

The effect of the width-to-length ratio on the sheet The curve of critical load – nonlinear deformation and the ratio of nonlinear to linear critical load for $\delta = 6$are given in Figure 6. With the sheet length remaining constant, the wider the sheet is, the lower the critical buckling load, while the higher the relative nonlinear deformation. According

to Figure 6 a, the linear buckling load for is $\frac{b}{a} = 1,2$ equal to $P_L = 11.23,4.634$ and doubling the width of the nanocomposite sheet has led to a 59% reduction in its critical linear buckling load.

Effect of transverse to longitudinal axial load ratio $\Delta = \gamma_y/\gamma_x$ load curve Critical - nonlinear deformation and ratio of nonlinear to linear critical load of sheet with dimensions: $\frac{h}{a} = 6$, $\frac{b}{a} = 2.5$It can be seen in Figure 7 . Linear buckling load in biaxial mode is 1.16 times uniaxial loading. But the way of loading did not affect the nonlinear behavior of the buckling.

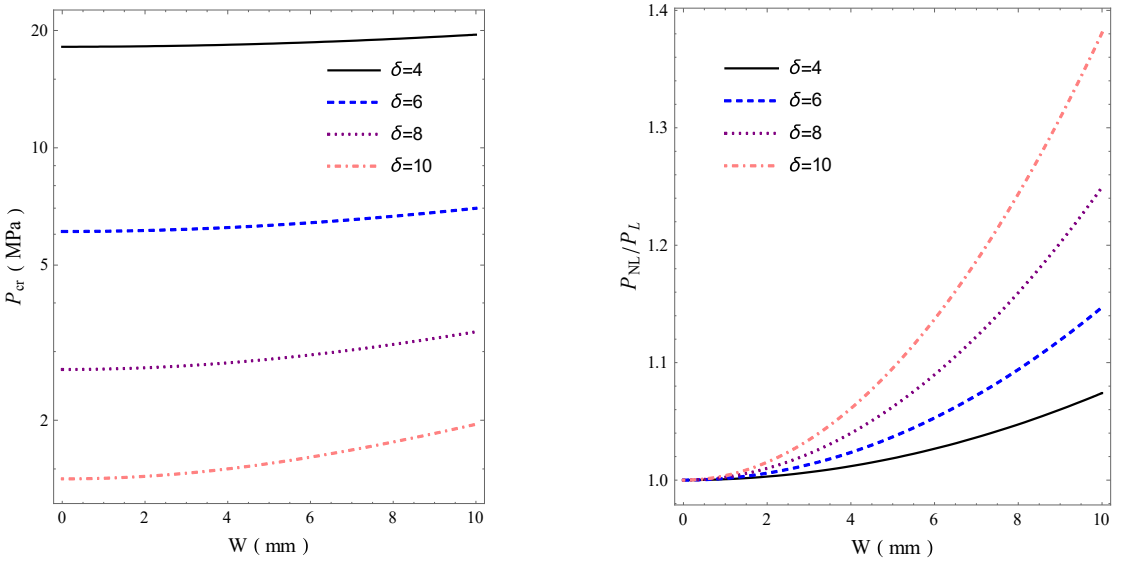

a **b**

Fig. 5. Effect of sheet thickness on: a(critical load curve - nonlinear deformation; b) Non-linear to linear critical load ratio

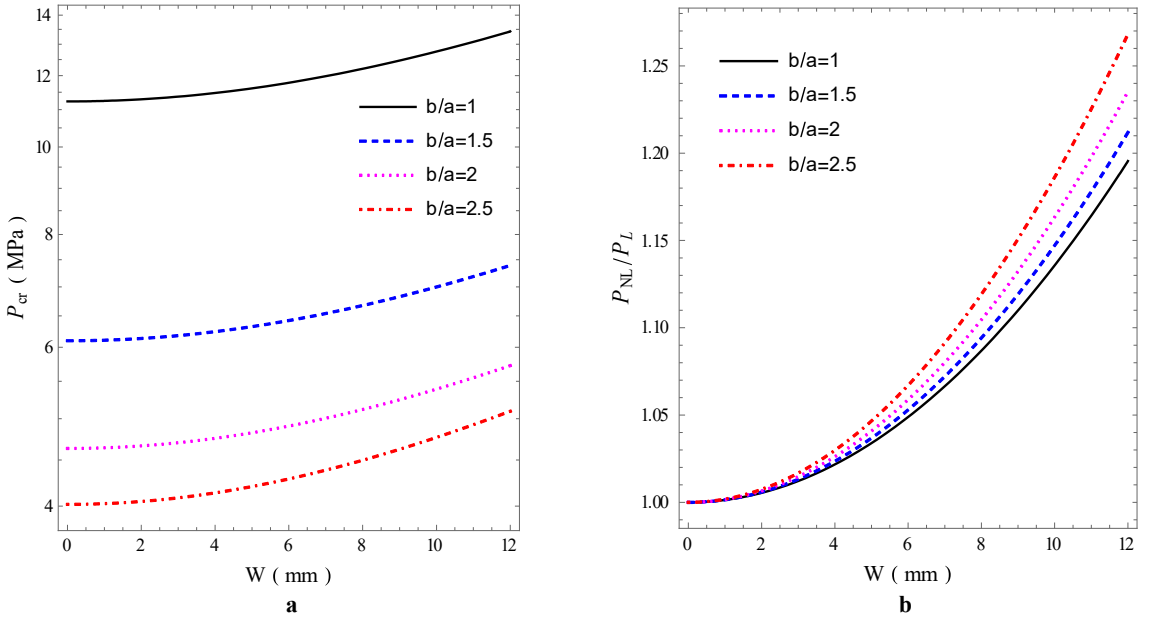

a **b**

Fig. 6. Effect of width to length ratio on: a) critical load curve - nonlinear deformation; b) Non-linear to linear critical load ratio

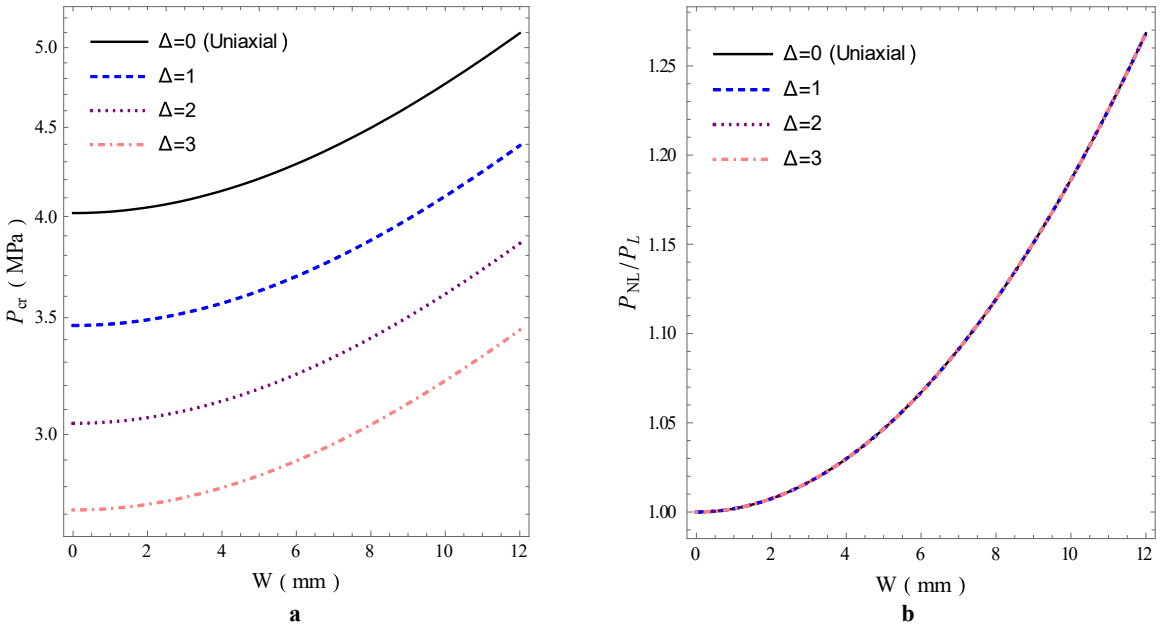

Fig. 7. Effect of transverse to longitudinal load ratio on: a) critical load curve - nonlinear deformation; b) Non-linear to linear critical load ratio

6. CONCLUSION

In this study, using the proposition of third-order shear deformation and Van Karman strain relations, the critical buckling load of rectangular composite plates reinforced with graphene nanosheets and in fully detailed boundary conditions has been obtained analytically and with the help of Navier method. In the following, the influence of colorful parameters, including amount and shape of graphene distribution, consistence and range graphene nanosheet, the rate of consistence to the length of the distance and its range has been studied on the buckling force.

The main results are:

- The presence of graphene has a great effect on the addition of the buckling load of the nanocomposite plate, so that with an increase of 0.5 of its mass, the direct buckling load has increased by 1/3.
- The nonlinear behavior in the distance with more graphene is less because the distance with an advanced mass chance of graphene is harder.
- The direct buckling load of symmetric distribution is1.72 and1.29 times the buckling load of asymmetric distribution and invariant distribution, respectively. On the other hand, the distance buckling of asymmetric distribution has the most nonlinear behavior with increasing strain.
- At a fixed length, increasing the thickness and decreasing the width of graphene were the factors that increased the critical buckling load.
- Doubling the consistency of the nanocomposite plate has led to a reduction in the critical buckling load by 85. Doubling the range of nanocomposite distance has led to a 59 reduction in its direct buckling critical load.

CONFLICTS OF INTEREST

The authors declare no conflict of interest.

REFERENCES

[1] Sun, Z., Hu, G., Nie, X., & Sun, J. (2022). An Analytical Symplectic Method for Buckling of Ring-Stiffened Graphene Platelet-Reinforced Composite Cylindrical Shells Subjected to Hydrostatic Pressure. Journal of

Marine Science and Engineering. https://doi.org/10.3390/jmse10121834

[2] Alazwari, M., Zenkour, A., & Sobhy, M. (2022). Hygrothermal Buckling of Smart Graphene/Piezoelectric Nanocomposite Circular Plates on an Elastic Substrate via DQM. Mathematics. https://doi.org/10.3390/math10152638

[3] Gunasekaran, V., Pitchaimani, J., & Chinnapandi, L. (2021). Acoustic radiation and transmission loss of FG-Graphene composite plate under nonuniform edge loading. European Journal of Mechanics - A/Solids. https://doi.org/10.1016/J.EUROMECHSOL.2021.104249

[4] Yang, Y., Chen, B., Lin, W., Li, Y., & Dong, Y. (2021). Vibration and symmetric thermal buckling of asymmetric annular sandwich plates with piezoelectric/GPLRC layers rested on foundation. Aerospace Science and Technology, 110, 106495. https://doi.org/10.1016/J.AST.2021.106495

[5] Javaheri, R., & Eslami, M. R. (2002). Buckling of functionally graded plates under in-plane compressive loading. ZAMM-Journal of Applied Mathematics and Mechanics / Zeitschrift für Angewandte Mathematik und Mechanik: Applied Mathematics and Mechanics, 82(4), 277-283. https://doi.org/10.1002/1521-4001(200204)82:4<277::AID-ZAMM277>3.0.CO;2-Y

[6] Asemi, K., Shariyat, M., Salehi, M., & Ashrafi, H. (2013). A full three-dimensional elasticity element for buckling analysis of FGM rectangular plates subjected to various combinations of biaxial normal and shear loads. Finite Elements in Analysis and Design, 74, 9-21. https://doi.org/10.1016/j.finel.2013.05.011

[7] Golmakani, M. E., & Zeighami, V. (2016). Buckling analysis of functionally graded carbon nanotube-reinforced composite plates using incremental loading and dynamic relaxation methods. Numerical Methods in Engineering, 35(1), 43-63. https://doi.org/10.18869/acadpub.jcme.35.1.43

[8] Zhao, W., & Kapania, R. K. (2016). Buckling analysis of unitized curvilinearly stiffened composite panels. Composite Structures, 135, 365-382. https://doi.org/10.1016/j.compstruct.2015.09.041.

[9] Qin, X. C., et al. (2017). Static and dynamic analyses of isogeometric curvilinearly stiffened plates. Applied Mathematical Modelling, 45, 336-364. https://doi.org/10.1016/j.apm.2016.12.035.

[10] Hao, P., et al. (2017). Isogeometric buckling analysis of composite variable-stiffness panels. Composite Structures, 165, 192-208. https://doi.org/10.1016/j.compstruct.2017.01.016.

[11] Zamani, R. (2015). Reinforcing effect of nanoclay on buckling behavior of nanocomposite grid shells: Experimental investigation. Modares Mechanical Engineering, 15(3), 411–418.

[12] Mohammadi Mehr, M., Mehrabi, M., & Shabani Nejad, E. (2018). Buckling and Vibration Analyses of Double-bonded Micro Composite Plates Reinforced by CNTs and BNNTs Based on MSGT. Persian, Amirkabir Journal of Mechanical Engineering, 50(5), 27-30.

[13] Melaibari, A., et al. (2020). Static stability of higher order functionally graded beam under variable axial load. Alexandria Engineering Journal, 59(3), 1661–1675. https://doi.org/10.1016/j.aej.2020.04.012.

[14] Karamanli, A., & Aydogdu, M. (2019). Buckling of laminated composite and sandwich beams due to axially varying in-plane loads. Composite Structures, 210, 391-408. https://doi.org/10.1016/j.compstruct.2018.11.067

[15] Dong, Y. H., et al. (2018). Buckling of spinning functionally graded graphene reinforced porous nanocomposite cylindrical shells: An analytical study. Aerospace Science and Technology, 82–83, 466-478. https://doi.org/10.1016/j.ast.2018.09.037.

[16] Zhou, Z., Ni, Y., Tong, Z., Zhu, S., Sun, J., & Xu, X. (2019). Accurate nonlinear buckling analysis of functionally graded porous graphene platelet reinforced composite cylindrical shells. International Journal of

Mechanical Sciences, 151, 537-550. https://doi.org/10.1016/j.ijmecsci.2018.12.012.

[17] Yazdani, S., Rust, WJ and Wriggers, P. (2016). Delamination growth in composite laminates of variable stiffness. International Journal for Numerical Methods in Engineering, 108(11), 1406-1424. https://doi.org/10.1002/nme.5264.

[18] Hao, P., Yuan, X., Liu, H., & Wang, B. (2017). Isogeometric buckling analysis of composite variable-stiffness panels. Composite Structures, 165, 192-208. https://doi.org/10.1016/j.compstruct.2017.01.016.

[19] Manickam, G., Bharath, A., Das, A.N., Chandra, A., & Barua, P. (2018). Thermal buckling behavior of variable stiffness laminated composite plates. Materials Today Communications, 16, 142-151. https://doi.org/10.1016/j.mtcomm.2018.05.003.

[20] Nguyen, N.V., Lee, J., & Nguyen-Xuan, H. (2019). Active vibration control of GPLs-reinforced FG metal foam plates with piezoelectric sensor and actuator layers. Composites Part B: Engineering, 172, 769-784. https://doi.org/10.1016/j.compositesb.2019.05.060.

[21] Bahaadini, R., Saidi, A.R., Arabjamaloei, Z., & Ghanbari-Nejad-Parizi, A. (2019). Vibration analysis of functionally graded graphene reinforced porous nanocomposite shells. International Journal of Applied Mechanics, 11(7). https://doi.org/10.1142/S1758825119500686.

[22] Rafiee, M.A., Rafiee, J., Wang, Z., & Koratkar, N. (2009). Enhanced mechanical properties of nanocomposites at low graphene content. ACS Nano, 3(12), 3884-3890. https://doi.org/10.1021/nn9010472.

[23] Zenkour, A.M. (2006). Generalized shear deformation theory for bending analysis of functionally graded plates. Applied Mathematical Modelling, 30(1), 67-84. https://doi.org/10.1016/j.apm.2005.03.009.